Multi-neutron emission of Cd isotopes

A. P. Severyukhin,[1,2] N. N. Arsenyev,[1] I. N. Borzov,[3,1] and E. O. Sushenok[1,2]
[1]*Bogoliubov Laboratory of Theoretical Physics, Joint Institute for Nuclear Research, 141980 Dubna, Moscow Region, Russia*
[2]*Dubna State University, Universitetskaya Street 19, 141982 Dubna, Moscow Region, Russia*
[3]*National Research Centre "Kurchatov Institute", 123182 Moscow, Russia*
(Received 6 November 2016; published 15 March 2017)

An influence of the phonon-phonon coupling (PPC) on the β-decay half-lives and multi-neutron emission probabilities is analyzed within the microscopic model based on the Skyrme interaction with tensor components included. The finite-rank separable approximation is used in order to handle large two-quasiparticle spaces. The even-even nuclei near the r-process paths at $N = 82$ are studied. The characteristics of ground states, 2^+ excitations, and β-decay strength of the neutron-rich Cd isotopes are treated in detail. It is shown that a strong redistribution of the Gamow-Teller strength due to the PPC is mostly sensitive to the multi-neutron emission probability of the Cd isotopes.

DOI: 10.1103/PhysRevC.95.034314

I. INTRODUCTION

β-decay properties are very important for understanding the nuclear structure evolution at extreme N/Z ratios, for analysis of radioactive ion-beam experiments, and modeling of the astrophysical r-process [1]. In the past years a renewed attention has been attracted to delayed multi-neutron emission (βxn) with $x = 2,3,\ldots$. The $\beta 2n$ emission was predicted in the early 1960s [2] and was later observed for the cases of ^{11}Li [3] and $^{30-32}$Na [4]. It was also considered for heavier nuclei in Ref. [5], emphasizing a competition between the sequential and resonant ("di-neutron") emission. Observation of the di-neutron emission in ^{16}Be decay was recently claimed [6] (see comment in Ref. [7] and discussion in Ref. [8]). Nowadays Bi isotopes in the mass region $N > 126$ are the heaviest nuclei where the delayed neutron emission has been studied [9].

A study of βxn processes facilitates developing a self-consistent approach based on the energy density functional (EDF). The process probability depends first on specific energy "landmarks": the β-decay energy release Q_β and neutron emission thresholds S_{xn}. An adequate description of these differential quantities poses constraints on the EDF in a high-isospin-asymmetry regime. The second crucial ingredient is the β-strength function: the spectral distribution of the β-decay matrix elements within the β-decay window (Q_β). Assuming an amplification of the intensity distribution by the integral Fermi factor, the most important contributions come from the allowed Gamow-Teller (GT) and high-energy first-forbidden (FF) β decays. Importantly, they should be treated by employing the one and the same self-consistent framework [10,11].

Experimental studies using the multipole decomposition analysis of the (n,p) and (p,n) reactions [12,13] found substantial GT strength above the GT resonance peak. This solves the longstanding problem of the missing experimental GT strength. Also it helps to overcome the discrepancies between the theoretical predictions using the one-phonon wave function of the quasiparticle random phase approximation (QRPA) and the measurements. It has been found necessary to take into account coupling with more complex configurations in order to shift some strength to higher transition energies in order to comply with the experimental results [14–16]. Using the Skyrme EDF and the random phase approximation (RPA), such attempts in the past [17,18] have allowed one to understand the damping of charge-exchange resonances and their particle decay. The damping of the GT mode was investigated using the Skyrme-RPA plus particle-vibration coupling [19]. The main difficulty is that complexity of the calculations increases rapidly with the size of the configurational space and one has to work within limited spaces. The separable form of the residual interaction is the practical advantage of the quasiparticle phonon model (QPM) [20], which allows one to perform the calculations in large configurational spaces [15,20,21]. The finite-rank separable approximation (FRSA) for the QRPA with Skyrme interactions [22,23] was invented to describe charge-exchange excitation modes [24,25].

In the present paper we concentrate on the delayed multi-neutron emission in the region below the neutron-rich doubly magic nucleus ^{132}Sn. The β-decay properties of r-process "waiting-point nuclei" ^{129}Ag, ^{130}Cd, and ^{131}In have attracted a lot of experimental efforts recently [26–30]. The theoretical analysis was done within the microscopic-macroscopic finite-range droplet model (FRDM+QRPA) [26,31], the continuum QRPA approach with the Fayans EDF (DF3+cQRPA) [10,11,32,33]. Recently, proton-neutron relativistic QRPA (pn-RQRPA) [34] and finite-amplitude method (FAM) [35] calculations have appeared. In general, the microscopic approaches [11,34,35] described the half-lives and total probabilities of the βxn emission better than the global approach [36] commonly used for astrophysical r-process modeling. Importantly, all the cited papers have used the one-phonon approximation. This may be not enough for adequate reproduction of the fine structure of the GT strength distribution near the neutron thresholds. Such a detailed analysis is feasible in the large-scale shell model [37] but this approach is limited by the number of available np-nh configurations.

In most of the cases, the experimental β-strength function is absent. In the combined analysis of integral β-decay characteristics, the half-lives and βxn-emission probabilities

 ©2017 American Physical Society

(P_{xn}) help to reconstruct the β-strength function. A ratio of P_{2n}/P_{1n} is a sensitive marker of the GT strength distribution in continuum. This carries back the information on the spin-isospin-dependent components of the EDF. The main aim of the present paper is to microscopically describe the change of the β-strength function profile caused by the 2p-2h fragmentation and to analyze its impact on the β-decay half-lives and βxn-emission rates in medium-heavy even-even Cd isotopes close to the $N = 82$ closed shell.

This paper is organized as follows. In Sec. II, we apply the FRSA model for studying the impact of the phonon-phonon coupling (PPC) effects on the delayed multi-neutron emission. In Sec. III we describe the important ingredients used in the P_{xn} calculations and, in particular, the Q_β value, the low-energy 2^+ excitations of the parent nucleus, and one- and two-neutron separation energies for the daughter nucleus. We analyze the results of the calculations of β-decay half-lives in Sec. IV A and the prediction of the βxn-emission probabilities in Sec. IV B. Conclusions are finally drawn in Sec. V.

II. β-DECAY CHARACTERISTICS WITHIN THE FRSA MODEL

The FRSA model for charge-exchange excitations and β decay was already introduced in Refs. [24,38] and in Refs. [25,39], respectively. In the present study of the β decay of even-even nuclei, this method is applied for the prediction of the βxn-emission probabilities.

The βxn emission is a multistep process consisting of (a) the β decay of the parent nucleus (N,Z) which results in feeding the excited states of the daughter nucleus $(N-1,Z+1)$ followed by the (b) βxn emissions to the ground state and/or (c) γ deexcitation to the ground state of the product nucleus $(N-1-X,Z+1)$. The starting point is the Hartree-Fock (HF)-BCS calculation [40] of the ground state within a spherical symmetry assumption. The continuous part of the single-particle spectrum is discretized by diagonalizing the HF Hamiltonian on a harmonic oscillator basis. In the particle-hole (p-h) channel we use the Skyrme interaction with the tensor components and their inclusion leads to the modification of the spin-orbit potential [41–43]. The pairing correlations are generated by the density-dependent zero-range force

$$V_{\text{pair}}(\mathbf{r}_1,\mathbf{r}_2) = V_0\left(1-\eta\left(\frac{\rho(r_1)}{\rho_0}\right)^\gamma\right)\delta(\mathbf{r}_1-\mathbf{r}_2), \tag{1}$$

where ρ_0 is the nuclear saturation density. The values of V_0, η, and γ are fixed to reproduce the odd-even mass difference of the studied nuclei [44,45]. To calculate binding energies of the daughter nucleus $B(N-1,Z+1)$ and the final nucleus $B(N-1-X,Z+1)$, the blocking of the BCS ground states [40,46] is taken into account. Finally, the calculated Q_β value and the neutron separation energies are given by

$$Q_\beta = \Delta M_{n-H} + B(Z+1,N-1) - B(Z,N), \tag{2}$$

$$S_{xn} = B(Z+1,N-1) - B(Z+1,N-1-X). \tag{3}$$

$\Delta M_{n-H} = 0.782$ MeV is the mass difference between the neutron and the hydrogen atom.

Constructing the QRPA equations on the basis of HF-BCS quasiparticle states of the parent (even-even) nucleus (N,Z) is the standard procedure [47]. The residual interactions in the p-h channel and the particle-particle channel are derived consistently from the Skyrme EDF. The eigenvalues of the QRPA equations are found numerically as the roots of the FRSA secular equation for the cases of electric excitations [22,44] and charge-exchange excitations [24,38]. It enables us to perform QRPA calculations in very large two-quasiparticle (2QP) spaces. In particular, the cutoff of the discretized continuous part of the single-particle spectra is performed at the energy of 100 MeV. This is sufficient for exhausting the Ikeda sum rule $S_- - S_+ = 3(N-Z)$. A rather complete list of FRSA features can be found in Ref. [25].

To take into account the PPC effects we follow the basic QPM ideas [15,20]. The Hamiltonian can be diagonalized in a space spanned by states composed of one or two QRPA phonons [25],

$$\Psi_\nu(JM) = \left(\sum_i R_i(J\nu)Q^+_{JMi} + \sum_{\lambda_1 i_1 \lambda_2 i_2} P^{\lambda_1 i_1}_{\lambda_2 i_2}(J\nu)\left[Q^+_{\lambda_1\mu_1 i_1}\bar{Q}^+_{\lambda_2\mu_2 i_2}\right]_{JM}\right)|0\rangle, \tag{4}$$

where λ denotes the total angular momentum and μ is its z projection in the laboratory system. The ground state of the parent nucleus (N,Z) is the QRPA phonon vacuum $|0\rangle$. The wave functions $Q^+_{\lambda\mu i}|0\rangle$ of the one-phonon excited states of the daughter nucleus $(N-1,Z+1)$ are described as linear combinations of 2QP configurations; $\bar{Q}^+_{\lambda\mu i}|0\rangle$ is a one-phonon electric excitation of the parent nucleus (N,Z). The normalization condition for the wave functions (4) is

$$\sum_i R_i^2(J\nu) + \sum_{\lambda_1 i_1 \lambda_2 i_2}\left(P^{\lambda_1 i_1}_{\lambda_2 i_2}(J\nu)\right)^2 = 1. \tag{5}$$

For the unknown amplitudes $R_i(J\nu)$ and $P^{\lambda_1 i_1}_{\lambda_2 i_2}(J\nu)$ the variational principle leads to the set of linear equations with rank equal to the number of one- and two-phonon configurations, and for its solution it is required to compute the Hamiltonian matrix elements coupling one- and two-phonon configurations [25,48]. The equations have the same form as the canonical QPM equations [15,20], where the single-particle spectrum and the residual interaction are derived from the same Skyrme EDF.

In the allowed GT approximation, the β^--decay rate is expressed by summing up the probabilities (in units of $G_A^2/4\pi$) of the energetically allowed transitions ($E_k^{\text{GT}} \leqslant Q_\beta$) weighted with the integrated Fermi function

$$T_{1/2}^{-1} = \sum_k \lambda^k_{if} = D^{-1}\left(\frac{G_A}{G_V}\right)^2 \times \sum_k f_0\left(Z+1,A,E_k^{\text{GT}}\right)B(GT)_k, \tag{6}$$

$$E_k^{\text{GT}} = Q_\beta - E_{1_k^+}, \tag{7}$$

where λ_{if}^{k} is the partial β^--decay rate, $G_A/G_V = 1.25$ is the ratio of the weak axial-vector and vector coupling constants, and $D = 6147$ s (see Ref. [49]). $E_{1_k^+}$ denotes the excitation energy of the daughter nucleus. As proposed in Ref. [50], this energy can be estimated by the following expression:

$$E_{1_k^+} \approx E_k - E_{2\mathrm{QP,lowest}}, \tag{8}$$

where E_k are the 1_k^+ eigenvalues of the QRPA equations, or of the equations taking into account the two-phonon configurations (4), and $E_{2\mathrm{QP,lowest}}$ corresponds the lowest 2QP energy. The spin-parity of the lowest 2QP state is, in general, different from 1^+. The wave functions allow us to determine GT transitions whose operator is $\hat{O}_- = f_q \sum_{i,m} t_-(i)\sigma_m(i)$, where f_q accounts for the quenching factor:

$$B(GT)_k = |\langle N-1, Z+1; 1_k^+|\hat{O}^-|N,Z;0_{gs}^+\rangle|^2. \tag{9}$$

Because of taking into account the tensor correlation effects within the 1p-1h and 2p-2h configurational spaces, any quenching factors are redundant [14], i.e., $f_q = 1$.

The difference in the characteristic time scales of the β decay and subsequent neutron emission processes justifies an assumption of their statistical independence. As proposed in Ref. [51], the P_{xn} probability of the βxn emission accompanying the β decay to the excited states in the daughter nucleus can be expressed as

$$P_{xn} = T_{1/2} D^{-1} \left(\frac{G_A}{G_V}\right)^2 \sum_{k'} f_0\left(Z+1, A, E_{k'}^{\mathrm{GT}}\right) B(GT)_{k'}, \tag{10}$$

where the GT transition energy ($E_{k'}^{\mathrm{GT}}$) is located within the neutron emission window $Q_{\beta xn} \equiv Q_\beta - S_{xn}$. For P_{1n} we have $Q_{\beta 2n} \leqslant E_{k'}^{\mathrm{GT}} \leqslant Q_{\beta n}$, while for P_{xn} this becomes $Q_{\beta x+1n} \leqslant E_{k'}^{\mathrm{GT}} \leqslant Q_{\beta xn}$. Since we neglect the γ deexcitation of the daughter nucleus, some overestimation of the resulting P_{xn} values can be obtained [11]. The study of the γ-deexcitation influence on the P_{xn} values within our approach is in progress.

III. DETAILS OF CALCULATIONS

As the parameter set in the particle-hole channel, we use the Skyrme EDF T43 which takes into account the tensor term [43]. The T43 set is one of 36 parametrizations, covering a wide range of the parameter space of the isoscalar and isovector tensor term added with refitting the parameters of the central interaction, where a fit protocol is very similar to that of the successful SLy parametrizations. The spin-isospin Landau parameter is given by

$$G_0' = -N_0\left[\frac{1}{4}t_0 + \frac{1}{24}t_3\rho^{\alpha_3} + \frac{1}{8}k_F^2(t_1 - t_2)\right], \tag{11}$$

where $N_0 = 2k_F m^*/\pi^2\hbar^2$ is the level density, with k_F being the Fermi momentum and m^* the nucleon effective mass. At saturation density ($\rho = \rho_0$), the T43 set predicts enough positive value for $G_0' = 0.14$ and it gives a reasonable description of properties of the GT and charge-exchange spin-dipole resonances [52]. Using the PPC effects within the FRSA model, the T43 set gives a reasonable agreement with experimental data for the β-decay half-life of the neutron-rich doubly magic nucleus ^{132}Sn; see Sec. IV A. It is worth mentioning that the first study of the strong impact of the tensor correlations on the ^{132}Sn half-life was done in Ref. [53].

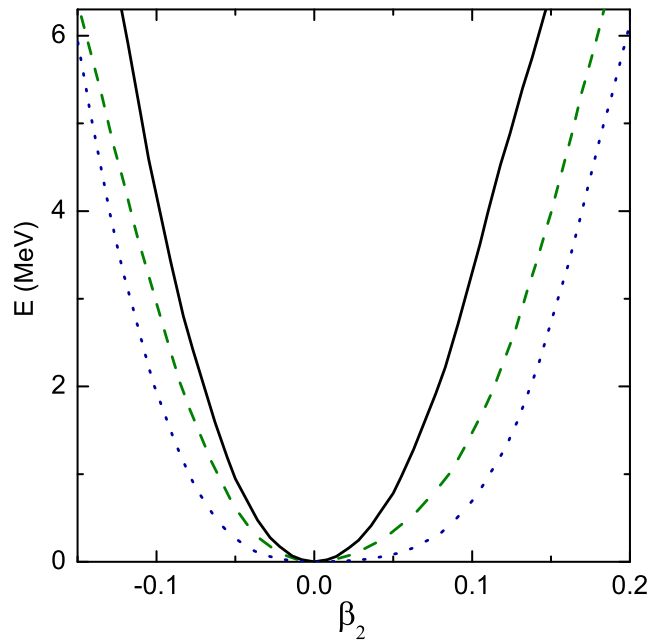

FIG. 1. Deformation energy curve as a function of the mass quadrupole deformation. The curves of ^{128}Cd, ^{130}Cd, and ^{132}Cd are denoted by the dashed, solid, and dotted lines, respectively.

The pairing correlations are generated by a surface-peaked pairing force (1) with $\eta = 1$, $\gamma = 1$, and the value $\rho_0 = 0.16$ fm $^{-3}$ for the nuclear saturation density. Using the soft cutoff at 10 MeV above the Fermi energies, the pairing strength is fixed to be $V_0 = -870$ MeV fm^3 in order to fit the experimental neutron pairing gaps of ^{126,128}Cd, ^{130}Sn, and ^{132}Te obtained by the three-point formula [24,38].

Spherical symmetry is imposed on the quasiparticle wave functions (QWFs). Keeping spherical symmetry might not be that bad in this mass region, and as an example we present the evolution of the deformation energies for ^{128,130,132}Cd. In Fig. 1, we show the HF-BCS energy curve obtained with a constraint on the the mass quadrupole moment Q_2 as a function of the dimensionless quadrupole deformation β_2:

$$\beta_2 = \sqrt{\frac{5}{16\pi}}\,\frac{4\pi\ Q_2}{3R^2A}, \tag{12}$$

where the radius constant is given by $R = 1.2A^{1/3}$ fm. The deformation energies are obtained using the EV8 code [54] that solves the HF-BCS equations for the same EDF via a discretization of the QWF on a three-dimensional Cartesian mesh. Our model for PPC effects on β-decay properties would probably be improved by the QWF generated by the EV8 calculations [54,55] with a single constraint on the axial mass quadrupole moment Q_2. The computational developments are still under way. A systematic comparison of the ratios of the calculated and experimental half-lives was done using both spherical and deformed QRPA calculations with the zero-range

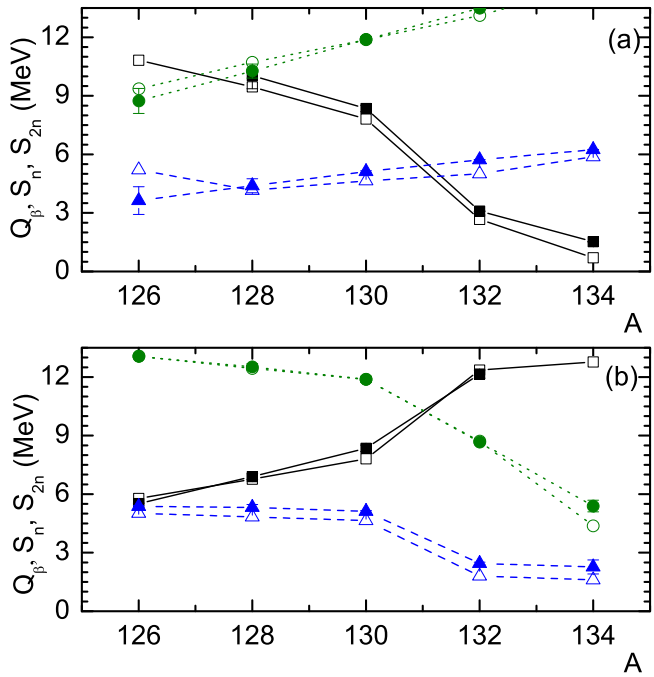

FIG. 2. Calculated β-decay windows Q_β of the parent nuclei (squares) and one- (triangles) and two-neutron (circles) separation energies for the daughter nuclei. The upper and lower panels correspond to the even $N = 82$ isotones and the even Cd isotopes, respectively. Results of the HF-BCS calculations are denoted by the open symbols. Experimental data (solid symbols) are taken from Ref. [58].

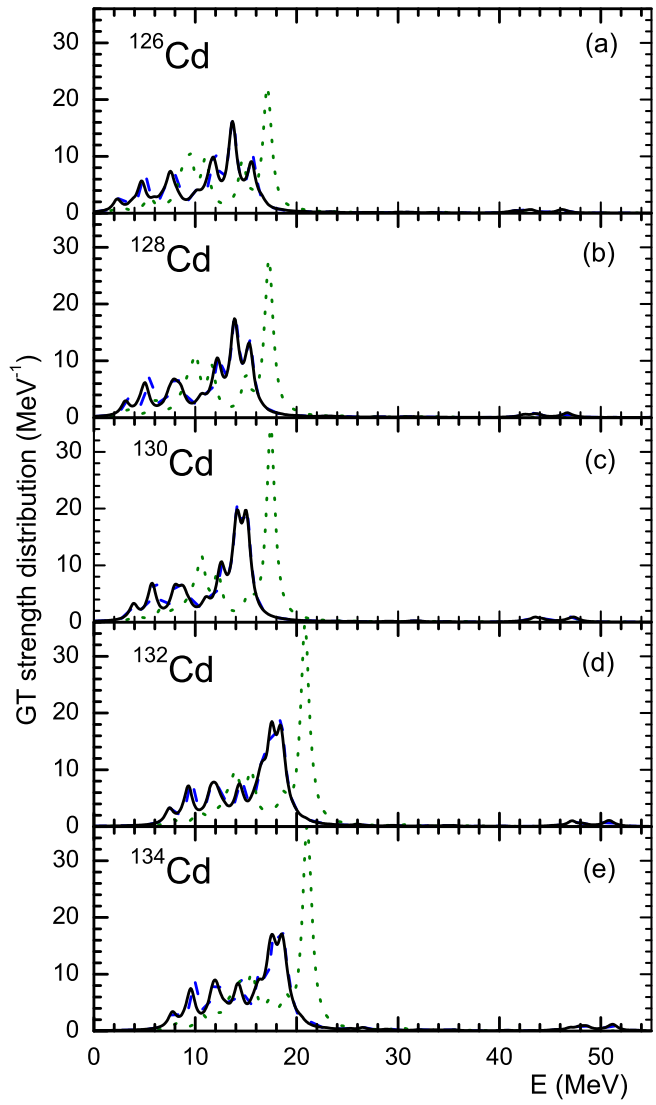

FIG. 3. GT strength distributions of $^{126-134}$Cd as functions of the excitation energy of the daughter nuclei. The QRPA calculations with the tensor interaction and without the tensor interaction are shown as dashed lines and dotted lines, respectively. The solid lines correspond to the quadrupole-phonon coupling effect on the QRPA results obtained with the tensor interaction.

nonlocal Skyrme interaction [56] and the finite-range Gogny force [57], showing that the inclusion of deformation improves significantly the description.

The correct description of the Q_β values for the parent nuclei and the neutron separation energies (S_{xn}) for the daughter nuclei is the important ingredient for the reliable prediction of the P_{2n}/P_{1n} ratios. The binding energies of the daughter and final nuclei are calculated with the blocking effect for unpaired nucleons [40,46]. For ^{126}Rh, ^{128}Ag, ^{126,128,130}In, ^{132}Sb, and ^{134}I, the neutron quasiparticle blocking is based on filling the $1h_{11/2}$ subshell, and the $2f_{7/2}$ subshell should be blocked for ^{132,134}In. The proton $1g_{9/2}$ and $1g_{7/2}$ subshells are chosen to be blocked in the cases of the Rh, Ag, and In isotopes and the Sb and I isotopes, respectively. The calculated Q_β, S_n, and S_{2n} values of the β decays of the even Cd isotopes and the $N = 82$ isotones are compared with the experimental data [58] in Fig. 2. The existing experimental data show a different A behavior, namely, the 6.6-fold reduction of Q_β values from ^{128}Pd to ^{134}Te and the gradual reduction of Q_β values with decreasing neutron number for the Cd isotopes. The results of the HF-BCS calculation with the T43 EDF are in a reasonable agreement with the experimental data.

To construct the wave functions (4) of the low-energy 1^+ states, in the present study we assume only the $[1_i^+ \otimes 2_{i'}^+]_{\rm QRPA}$ terms for separating the sole impact of the quadrupole-phonon coupling. All one- and two-phonon configurations with the excitation energy of the daughter nucleus, $E_{1_k^+}$, up to 16 MeV are included. We have checked that the inclusion of the high-energy configurations leads to minor effects on the half-life values. As it is pointed out in Ref. [25], the $[1_1^+ \otimes 2_1^+]_{\rm QRPA}$ configuration is the important ingredient for the half-life description since the $[2_1^+]_{\rm QRPA}$ state is the lowest collective excitation which leads to the minimal two-phonon energy and the maximal Hamiltonian matrix elements for coupling of the one- and two-phonon configurations.

First we examine the role of the tensor interactions on QRPA calculations. In Fig. 3, the GT strength distributions of $^{126-134}$Cd are averaged out by a Lorentzian distribution of 1 MeV width. All calculations are without any quenching factor. The excitation energies refer to the ground state of the daughter nucleus. The inclusion of the tensor interaction

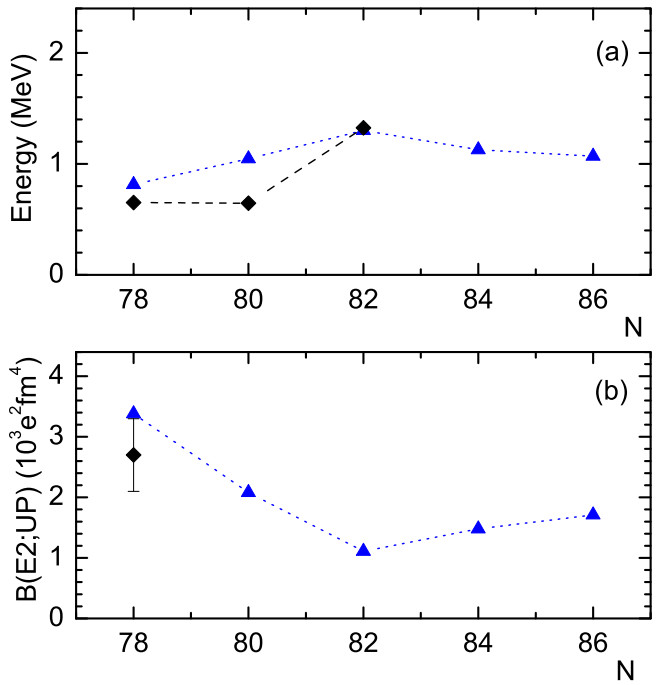

FIG. 4. Energies and $B(E2)$ values for up-transitions to the $[2_1^+]_{\rm QRPA}$ states in the neutron-rich Cd isotopes. Results of the QRPA calculations are denoted by the triangles. Experimental data (diamonds) are taken from Refs. [59–61].

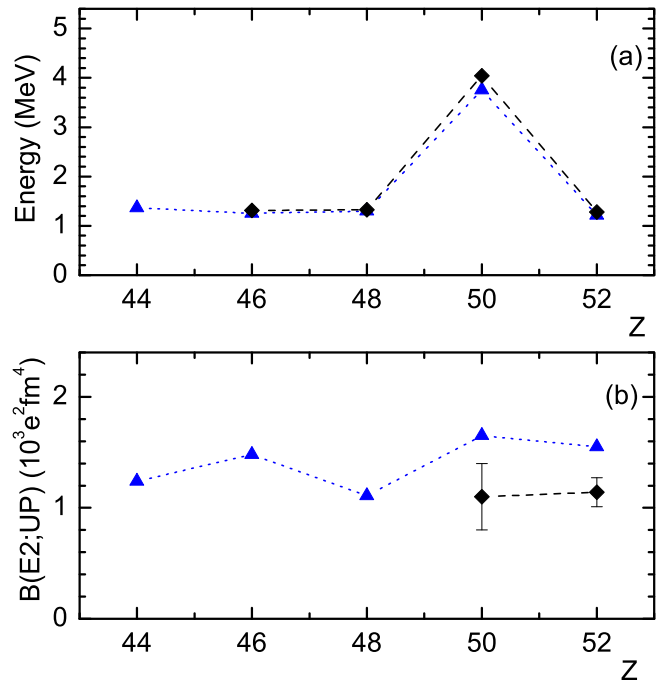

FIG. 5. Same as Fig. 2, but for the neutron-rich $N = 82$ isotones. Experimental data (diamonds) are taken from Refs. [59,62–64].

leads to a noticeable redistribution of the GT strength. One can see that part of the strength is fragmented in the low-energy peaks and also small high-energy peaks above $E_x = 40$ MeV. Including the two-phonon configurations leads to further increase of this effect and to the appearance of the weak fragmented satellites at low transition energy (see Sec. IV). It is seen that the quadrupole-phonon coupling plays a minor role for the GT resonance fragmentation. This probably points to a deficiency of our model space rather than to a particular problem due to the EDF. More careful study of the GT resonance properties is planned as a future work. Note that hereafter we discuss the results obtained with the tensor interaction.

It is interesting to examine the energies and transition probabilities of the $[2_1^+]_{\rm QRPA}$ states of the neutron-rich Cd isotopes (see Fig. 4). There is a significant increase of the 2_1^+ energy of ^{130}Cd. It corresponds to a standard evolution of the 2_1^+ energy near closed shells. In all five nuclei, the 2_1^+ wave functions are dominated by the proton configuration $\{1g_{9/2},1g_{9/2}\}_\pi$ (>73%). The closure of the neutron subshell $1h_{11/2}$ in ^{130}Cd leads to the vanishing of the neutron pairing and as a result the lowest neutron 2QP energy $\{2f_{7/2},1h_{11/2}\}_\nu$ is larger than the lowest neutron 2QP energies $\{1h_{11/2},1h_{11/2}\}_\nu$ in ^{128}Cd and $\{2f_{7/2},2f_{7/2}\}_\nu$ in ^{132}Cd. Correspondingly the 2_1^+ state of ^{130}Cd has noncollective structure with the $\{1g_{9/2},1g_{9/2}\}_\pi$ domination (about 96%) and the $B(E2)$ value is reduced. Because the data for the Cd isotopes are very scarce, the $N = 82$ isotones are used for reference. Results of QRPA calculation with T43 EDF and the experimental data [59,62–64] are shown in Fig. 5. The calculated values are in a reasonable agreement with the data. Moving along the neutron-rich $N = 82$ isotones chain one can find that 2_1^+ states in ^{126}Ru, ^{128}Pd, and ^{130}Cd, as is discussed above, have a noncollective structure with a domination of the $\{1g_{9/2},1g_{9/2}\}_\pi$ configuration. In ^{132}Sn, the main configurations are the neutron $\{2f_{7/2},1h_{11/2}\}_\nu$ (56%) and the proton $\{2d_{5/2},1g_{9/2}\}_\pi$ (37%) ones. In ^{134}Te, the 2_1^+ state is dominated by the lowest 2QP component $\{1g_{7/2},1g_{7/2}\}_\pi$. The structure peculiarities are reflected in the $B(E2)$ behavior in this chain. We find a satisfactory description of the isotonic dependence of the 2_1^+ energy near the closed proton shell.

IV. RESULTS

Using the same set of parameters, the main features of the β-decay and available βxn rates are described for the neutron-rich nuclei $^{132}_{50}$Sn, $^{126,128,130,132,134}_{48}$Cd, $^{128}_{46}$Pd, and $^{126}_{44}$Ru. The integral β-decay observables are substantially defined by the structure of the β-strength function. Figure 6 depicts the β-strength function of ^{130,132}Cd (in terms of the transition rate) calculated within the QRPA [Figs. 6(a) and 6(c)] and with the $[1_i^+ \otimes 2_{i'}^+]_{\rm QRPA}$ configurations taken into account [Figs. 6(b) and 6(d)].

For ^{130}Cd, the QRPA strength function has a rather simple two-peak structure; the main transition to the $[1_1^+]_{\rm QRPA}$ state is built on the $\{\pi 1g_{9/2},\nu 1g_{7/2}\}$ configuration. Inclusion of the PPC shifts the main peak by +120 keV, increasing its amplitude by 5%, and also an additional low rate peak at $E_2^{\rm GT} = 2.4$ MeV comes from the $[1_1^+ \otimes 2_1^+]_{\rm QRPA}$ configuration (93%). Thus an additional peak is dominated by the four-quasiparticle configuration $\{\pi 1g_{9/2},\pi 1g_{9/2},\pi 1g_{9/2},\nu 1g_{7/2}\}$. However, the main contribution to the GT matrix element

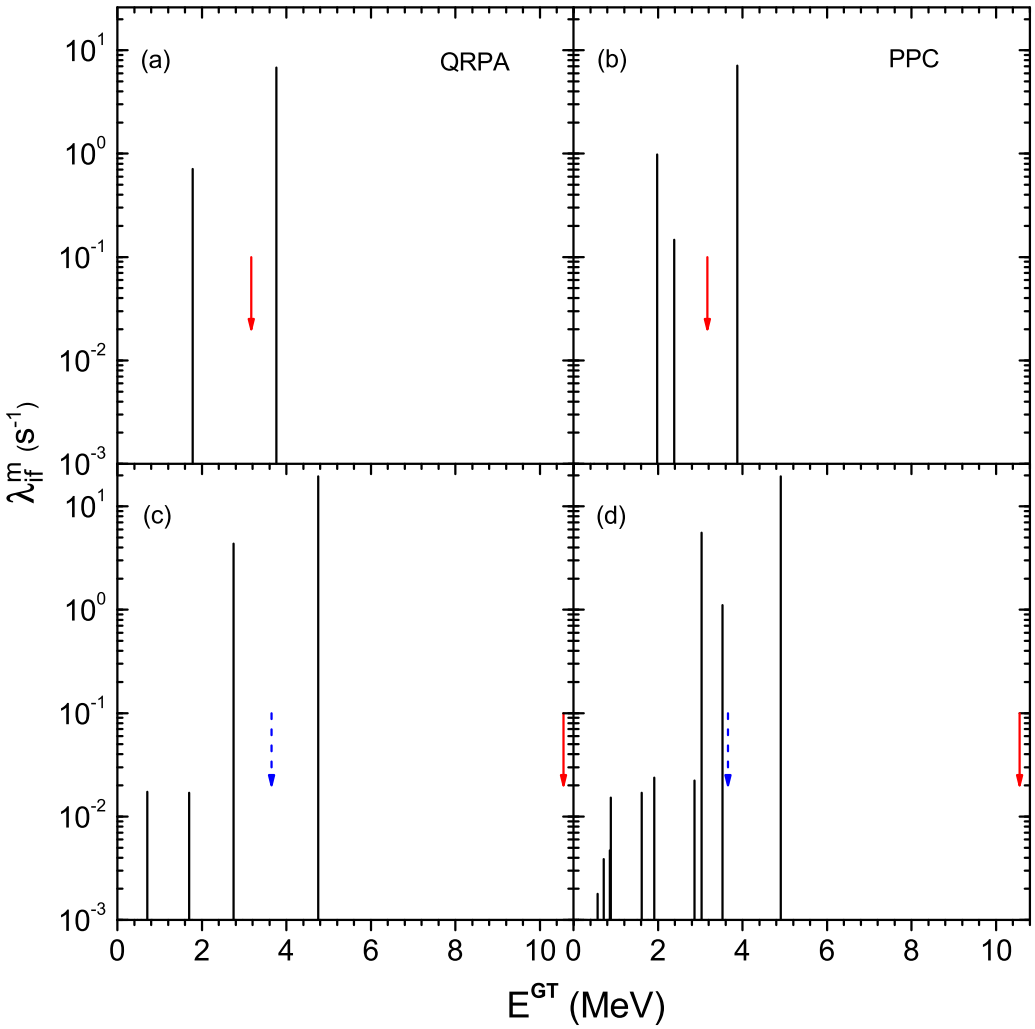

FIG. 6. The phonon-phonon coupling effect on the β-transition rates in ^{130}Cd (top) and ^{132}Cd (bottom). The left and right panels correspond to the calculations within the QRPA and taking into account the $[1^+_i \otimes 2^+_{i'}]_{\rm QRPA}$ configurations, respectively. The calculated $Q_{\beta 1n}$ and $Q_{\beta 2n}$ energies are denoted by the solid and dashed arrows, respectively.

comes from the one-phonon configuration $[1^+_1]_{\rm QRPA}$ which exhausts about 6% of the 1^+_2 wave function. These changes are translated into the corresponding half-life reduction and $P_{\rm tot}$ growth. This is discussed in the next sections. As can be seen from Fig. 6, we get the similar tendency of the QRPA strength function in the case of ^{132}Cd. However, there are remarkable changes in the values of the $Q_{\beta 1n}$ and $Q_{\beta 2n}$ windows. It is seen that the calculated neutron-emission probability ($P_{\rm tot}$) exhausts 100% since all the GT transition energies are less than $Q_{\beta 1n}$. The additional (two-phonon) peak leads to the P_{2n}/P_{1n} increase; see Sec. IV B.

A. β-decay half-lives

For ^{126,128,130,132,134}Cd, the results of our calculations and experimental data [28] are shown in Table I. First, the half-lives are studied within the one-phonon approximation. We assume the allowed GT approximation and neglect the γ deexcitation of the daughter nucleus. This means that the P_{xn} values calculated in the one-phonon approximation are not sensitive to the GT quenching factor; see Eq. (10). But the GT quenching-factor effect leads to an increase of the QRPA half-life. Columns $f_q = 1$ and $f_q < 1$ give QRPA

TABLE I. The quadrupole-phonon coupling effect on β-decay half-lives of the neutron-rich Cd isotopes. The QRPA half-life is calculated with the GT quenching factor or without ($f_q = 1$). See text for more details. All the calculations take into account the tensor terms of the T43 EDF. Experimental data are taken from Ref. [28].

Nucleus	Half-life (ms)			
	QRPA		PPC	Expt.
	$f_q = 1$	$f_q < 1$		
^{126}Cd	334	398	263	513 ± 6
^{128}Cd	212	227	180	245 ± 5
^{130}Cd	133	139	121	127 ± 2
^{132}Cd	42	44	38	82 ± 4
^{134}Cd	36	38	32	65 ± 15

half-lives calculated without and with the quenching factor, respectively. The quenching factor mimics the GT strength in the Q_β window, which appears in the PPC calculation. In such a prescription f_q is slightly dependent on the mass number; namely, for $^{126-134}$Cd it changes from 0.92 to 0.98 correspondingly. At a qualitative level, our results reproduce the experimental mass dependence of the half-lives. The largest contribution (>80%) in all the calculated half-lives comes from the $[1_1^+]_{\rm QRPA}$ state. The dominant configuration of the $[1_1^+]_{\rm QRPA}$ states is $\{\pi 1g_{9/2}, \nu 1g_{7/2}\}$ with the contribution of about 99%, and $\log ft \approx 2.9$ in all the Cd isotopes considered. Let us consider how to explain the 3.2-fold reduction of calculated half-life values from ^{130}Cd to ^{132}Cd; see Table I. The $\{\pi 1g_{9/2}, \nu 1g_{7/2}\}$ energy is equal to 7.5 MeV for ^{130}Cd and 9.5 MeV for ^{132}Cd. Also we find that the lowest 2QP energy is either the $\{\pi 1g_{9/2}, \nu 1h_{11/2}\}$ value of 3.4 MeV for ^{130}Cd or the $\{\pi 1g_{9/2}, \nu 2f_{7/2}\}$ value of 1.9 MeV for ^{132}Cd. As a result, the excitation energy of the first 1^+ state is increased from ^{130}In to ^{132}In. Therefore, the 4.6 MeV increase of the Q_β values (see Fig. 2) plays the key role in explaining this half-life reduction. The analysis within the one-phonon approximation can help to explain the main peculiarities of the half-lives' A dependence, but it is only a rough estimate.

Let us now discuss the extension of the space to one- and two-phonon configurations on the half-lives. As expected, the largest contribution (>70%) in half-life comes from the 1_1^+ state calculated with the PPC. The dominant contribution in the wave function of the first 1^+ state comes from the $[1_1^+]_{\rm QRPA}$ configuration, but the $[1_1^+ \otimes 2_1^+]_{\rm QRPA}$ contribution is appreciable. Inclusion of the two-phonon terms results in a decrease of the 1_1^+ energy. The well-known experimental characteristics of the 1_1^+ state in ^{130}In is a stringent test for the existing microscopic approaches [65]. Results of the FRSA model with the T43 EDF ($E_{1_1^+} = 3.9$ MeV and $\log ft = 3.0$) can be compared with the experimental excitation energy $E_{1_1^+} = 2.12$ MeV and $\log ft = 4.1$ [27]. The calculated two-quasiparticle energy and unperturbed $B(GT)$ value are too large to be properly renormalized in the inclusion of the two-phonon configurations. One may possibly seek for improvements of the $T = 0$ pairing term in the EDF used. Table I shows the half-life reduction as an effect of the quadrupole-phonon coupling; see, e.g., Fig. 6. The calculated half-life of ^{130}Cd is in excellent agreement with the experimental data [28]. For ^{132,134}Cd, the calculated half-lives are shorter than that measured in Ref. [28]. In fact, for $N > 82$ one has also to assume an increased role of the FF transitions, which would further reduce the total half-lives. According to Ref. [66], the contributions of the FF transitions to the total half-lives are 7.0%, 20.5%, and 39.0%, while in Ref. [34] they are 11.755%, 39.199%, and 48.951% for ^{130,132,134}Cd correspondingly. Thus, the present discrepancies between the measured and calculated half-lives of ^{132,134}Cd cannot be assigned to neglect of the FF transitions.

It is worth mentioning that the EDF T43 within the QRPA gives a satisfactory agreement with experimental data for the β-decay half-life of the neutron-rich doubly magic nucleus ^{132}Sn [53]. The PPC effect results in an improvement of the half-life description; see Fig. 7. As can be seen from Table I and Fig. 7, there are different behaviors of the existing experimental half-lives [28,67], namely, the 313-fold reduction of half-life values from $^{132}_{50}$Sn to $^{130}_{48}$Cd and the gradual reduction of half-lives with increasing neutron number for ^{126,128,130}Cd. One can see that the FRSA model with the T43 EDF reproduces this behavior and our results predict the half-lives for $^{128}_{46}$Pd and $^{126}_{44}$Ru. Furthermore, an improvement can be achieved if the FF transitions are taken into account [10]. It is planned to extend our formalism to include the FF transitions.

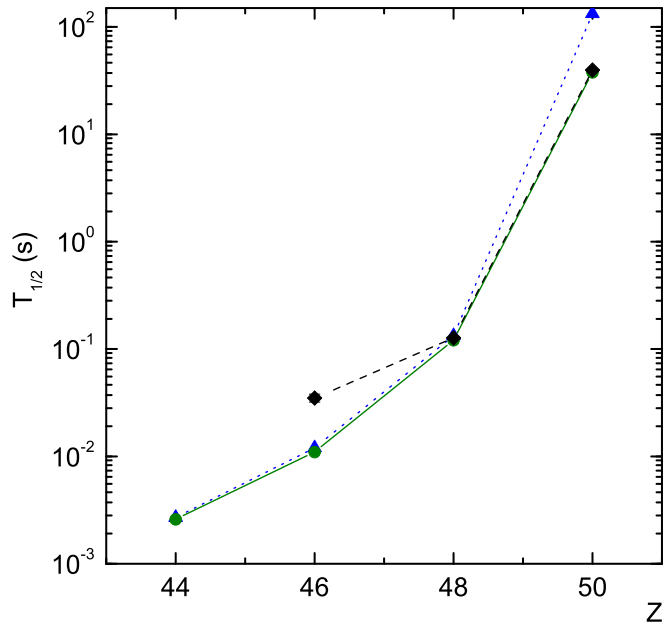

FIG. 7. The phonon-phonon coupling effect on β-decay half-lives of the neutron-rich $N = 82$ isotones. The circles correspond to the half-lives calculated with inclusion of the $[1_i^+ \otimes 2_{i'}^+]_{\rm QRPA}$ configurations; the triangles are the QRPA calculations. Experimental data (diamonds) are from Refs. [28,67].

B. Probabilities of the β-delayed neutron emission

Additional constraints on the β-strength function are given by the total and multi-neutron emission probabilities. The well-known experimental probabilities are $P_{\rm tot} = 3.5 \pm 1.0\%$ for ^{130}Cd [27] and $60 \pm 15\%$ for ^{132}Cd [26]. The calculated $P_{1n,2n}$ values are displayed in Fig. 8. For ^{126}Cd, one has to mention a nonzero $P_{\rm tot}$ value less than 1%. It is worth pointing out that the nonzero probability of the neutron emission was also predicted within the pn-RQRPA before [34]. For ^{130}Cd, the calculated $P_{\rm tot}$ value of 13.7% is higher than the experimental value of 3.5% [27], which may indicate the necessity of including the $T = 0$ pairing interaction. For all considered isotopes we obtain the maximal P_{1n} and P_{2n} values in the case of ^{132}Cd. The redistribution of the QRPA estimate in favor of P_{2n} occurs when the PPC effect is included: $P_{2n} = 25.6\%$ compared to $P_{1n} = 74.4\%$. This differs from the DF3a+cQRPA prediction by Ref. [66], which gives $P_{1n} = 84.13\%$ and $P_{2n} = 0.14\%$. Also, it is interesting to compare the P_{2n}/P_{1n} ratios. They are 0.002 in Ref. [66] and 0.34 in the present calculation. The difference between the predictions of

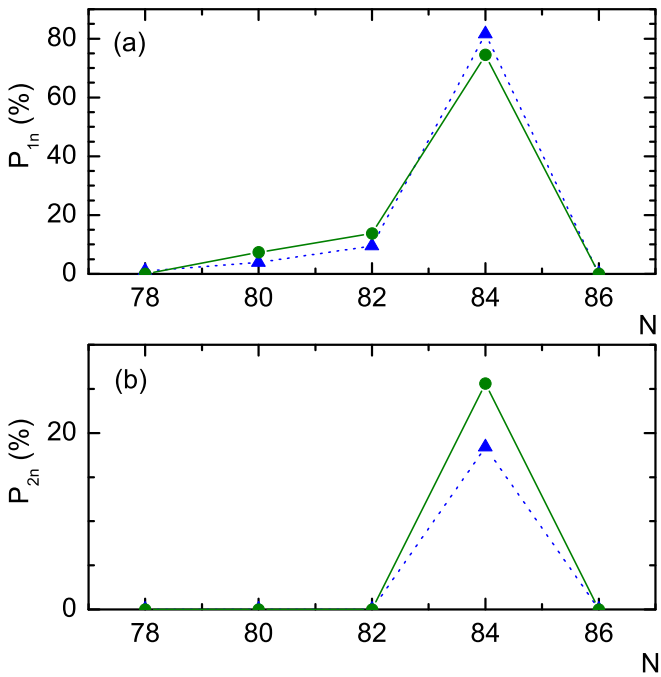

FIG. 8. The phonon-phonon coupling effect on β-delayed neutron-emission probabilities of the neutron-rich Cd isotopes. The circles correspond to the probabilities calculated with inclusion of the $[1_i^+ \otimes 2_{i'}^+]_{\rm QRPA}$ configurations; the triangles are the QRPA calculations.

two models can be explained by the sensitivity of multi-neutron delayed emission to the details of the β-strength function and the neutron separation energies. Also, farther from the closed shell (^{134}Cd) one cannot neglect the increasing contribution of the FF transition known to reduce the $P_{\rm tot}$ value [11,33,66] and substantially redistributing P_{xn} values. As is shown in Ref. [66], the DF3a+cQRPA calculation gives $P_{1n} = 32.75\%$, $P_{2n} = 47.47\%$, and $P_{3n} = 7.12\%$. The values $P_{1n} = 50.9\%$, $P_{2n} = 3.1\%$, and $P_{3n} = 0.5\%$ are obtained within the pn-RQRPA [34]. The phenomenological model [68], taking into account the γ deexcitation of the daughter nucleus, predicts that the dominating channel should be βn emission, and the corresponding probabilities are $P_{1n} = 71.7\%$ and $P_{2n} = 4.1\%$ for ^{134}Cd.

It would be instructive to study the PPC effect on the $P_{1n,2n}$ values of the neutron-rich nuclei. For ^{126,128,130}Cd within the QRPA there are two main GT decays which define the $P_{\rm tot}$ values (see, for example, Fig. 8). The inclusion of the PPC has a stronger influence on the energy shift of the 1_3^+ state which is mainly built on the $[1_2^+]_{\rm QRPA}$ configuration. Also the two-phonon state 1_2^+ appears. Both effects increase the $P_{\rm tot}$ value. In the case of ^{132}Cd these dynamic features of 1_2^+ and 1_3^+ states are responsible for increasing the P_{2n} value. The QRPA value $P_{2n}/P_{1n} = 0.22$ is replaced by 0.34 with the PPC included. Notice that $P_{2n}/P_{1n} = 0.29$ if the 1_2^+ state is not taken into account.

V. CONCLUSIONS

Starting from the Skyrme mean-field calculations, we studied the effects of the phonon-phonon coupling on the properties of the β-delayed multi-neutron emission and, in particular, on P_{2n}/P_{1n} ratios of nuclei in the mass range $A \approx 130$. The finite-rank separable approach to the QRPA problem enables one to perform the calculations in very large configurational spaces.

The T43 parametrization of the Skyrme interaction is used for all calculations in connection with the surface-peaked zero-range pairing interaction. In particular, we study the multi-neutron emission in ^{132}Cd in comparison with $N = 82$ isotone ^{130}Cd. We found a significant two-neutron emission for ^{132}Cd, the effect which was predicted within the FRDM+QRPA and the DF3+cQRPA before. Notice that, as well as in the DF3+cQRPA calculations, our results from the Skyrme interaction are in reasonable agreement with experimental half-lives. It is the first successful description obtained with the Skyrme interaction for the experimental neutron-emission probabilities. The coupling between one- and two-phonon terms in the wave functions of 1^+ states is shown to be essential. The QRPA underestimates the P_{2n}/P_{1n} values. Inclusion of the two-phonon configurations produces an impact on the P_{2n} value which leads to the 55% increase of the P_{2n}/P_{1n} ratio. For ^{126,128,130,132,134}Cd, the maximal P_{1n} and P_{2n} values are obtained in the case of ^{132}Cd. For ^{126}Cd, a nonzero probability of the neutron emission is found.

We conclude that the present approach makes it possible to perform the new microscopic analysis of the rates of the β-delayed multi-neutron emission. The model can be extended by enlarging the variational space for the 1^+ states with the inclusion of the two-phonon configurations constructed from phonons with monopole, dipole, and octupole multipolarities. The computational developments that would allow us to conclude on this point are under way.

ACKNOWLEDGMENTS

We thank Nguyen Van Giai, Yu. E. Penionzhkevich, H. Sagawa, and D. Verney for useful discussions. This work is supported by the Russian Science Foundation (Grant No. RSF-16-12-10161).

[1] K. Langanke and G. Martínez-Pinedo, Rev. Mod. Phys. **75**, 819 (2003).
[2] V. I. Goldansky, Nucl. Phys. **19**, 482 (1960).
[3] R. E. Azuma, L. C. Carraz, P. G. Hansen, B. Jonson, K.-L. Kratz, S. Mattsson, G. Nyman, H. Ohm, H. L. Ravn, A. Schröder, and W. Ziegert, Phys. Rev. Lett. **43**, 1652 (1979).
[4] C. Detraz, M. Epherre, D. Guillemaud, P. G. Hansen, B. Jonson, R. Klapisch, M. Langevin, S. Mattsson, F. Naulin, G. Nyman, A. M. Poskanzer, H. L. Ravn, M. de Saint-Simon, K. Takahashi, C. Thibault, and F. Touchard, Phys. Lett. B **94**, 307 (1980).
[5] Yu. S. Lyutostansky, V. K. Sirotkin, and I. V. Panov, Phys. Lett. B **161**, 9 (1985).

[6] A. Spyrou, Z. Kohley, T. Baumann, D. Bazin, B. A. Brown, G. Christian, P. A. DeYoung, J. E. Finck, N. Frank, E. Lunderberg, S. Mosby, W. A. Peters, A. Schiller, J. K. Smith, J. Snyder, M. J. Strongman, M. Thoennessen, and A. Volya, Phys. Rev. Lett. **108**, 102501 (2012).

[7] F. M. Marqués, N. A. Orr, N. L. Achouri, F. Delaunay, and J. Gibelin, Phys. Rev. Lett. **109**, 239201 (2012).

[8] C. A. Bertulani and V. Zelevinsky, Nature (London) **532**, 448 (2016).

[9] R. Caballero-Folch, C. Domingo-Pardo, J. Agramunt, A. Algora, F. Ameil, A. Arcones, Y. Ayyad, J. Benlliure, I. N. Borzov, M. Bowry, F. Calviño, D. Cano-Ott, G. Cortés, T. Davinson, I. Dillmann, A. Estrade, A. Evdokimov, T. Faestermann, F. Farinon, D. Galaviz, A. R. García, H. Geissel, W. Gelletly, R. Gernhäuser, M. B. Gómez-Hornillos, C. Guerrero, M. Heil, C. Hinke, R. Knöbel, I. Kojouharov, J. Kurcewicz, N. Kurz, Yu. A. Litvinov, L. Maier, J. Marganiec, T. Marketin, M. Marta, T. Martínez, G. Martínez-Pinedo, F. Montes, I. Mukha, D. R. Napoli, C. Nociforo, C. Paradela, S. Pietri, Zs. Podolyák, A. Prochazka, S. Rice, A. Riego, B. Rubio, H. Schaffner, Ch. Scheidenberger, K. Smith, E. Sokol, K. Steiger, B. Sun, J. L. Taín, M. Takechi, D. Testov, H. Weick, E. Wilson, J. S. Winfield, R. Wood, P. Woods, and A. Yeremin, Phys. Rev. Lett. **117**, 012501 (2016).

[10] I. N. Borzov, Phys. Rev. C **67**, 025802 (2003).

[11] I. N. Borzov, Phys. Rev. C **71**, 065801 (2005).

[12] T. Wakasa, H. Sakai, H. Okamura, H. Otsu, S. Fujita, S. Ishida, N. Sakamoto, T. Uesaka, Y. Satou, M. B. Greenfield, and K. Hatanaka, Phys. Rev. C **55**, 2909 (1997).

[13] M. Ichimura, H. Sakai, and T. Wakasa, Prog. Part. Nucl. Phys. **56**, 446 (2006).

[14] G. F. Bertsch and I. Hamamoto, Phys. Rev. C **26**, 1323 (1982).

[15] V. A. Kuzmin and V. G. Soloviev, J. Phys. G **10**, 1507 (1984).

[16] S. Drozdz, F. Osterfeld, J. Speth, and J. Wambach, Phys. Lett. B **189**, 271 (1987).

[17] G. Coló, Nguyen Van Giai, P. F. Bortignon, and R. A. Broglia, Phys. Rev. C **50**, 1496 (1994).

[18] G. Coló, H. Sagawa, Nguyen Van Giai, P. F. Bortignon, and T. Suzuki, Phys. Rev. C **57**, 3049 (1998).

[19] Y. F. Niu, G. Colò, M. Brenna, P. F. Bortignon, and J. Meng, Phys. Rev. C **85**, 034314 (2012).

[20] V. G. Soloviev, *Theory of Atomic Nuclei: Quasiparticles and Phonons* (Institute of Physics, Bristol, U.K., 1992).

[21] V. A. Kuzmin and V. G. Soloviev, J. Phys. G **11**, 603 (1985).

[22] Nguyen Van Giai, Ch. Stoyanov, and V. V. Voronov, Phys. Rev. C **57**, 1204 (1998).

[23] A. P. Severyukhin, V. V. Voronov, and Nguyen Van Giai, Eur. Phys. J. A **22**, 397 (2004).

[24] A. P. Severyukhin, V. V. Voronov, and Nguyen Van Giai, Prog. Theor. Phys. **128**, 489 (2012).

[25] A. P. Severyukhin, V. V. Voronov, I. N. Borzov, N. N. Arsenyev, and Nguyen Van Giai, Phys. Rev. C **90**, 044320 (2014).

[26] M. Hannawald, V. N. Fedoseyev, U. Köster, K.-L. Kratz, V. I. Mishin, W. F. Mueller, H. L. Ravn, J. Van Roosbroeck, H. Schatz, V. Sebastian, and W. B. Walters (the ISOLDE Collaboration), Nucl. Phys. A **688**, 578c (2001).

[27] I. Dillmann, K.-L. Kratz, A. Wöhr, O. Arndt, B. A. Brown, P. Hoff, M. Hjorth-Jensen, U. Köster, A. N. Ostrowski, B. Pfeiffer, D. Seweryniak, J. Shergur, and W. B. Walters (the ISOLDE Collaboration), Phys. Rev. Lett. **91**, 162503 (2003).

[28] G. Lorusso, S. Nishimura, Z. Y. Xu, A. Jungclaus, Y. Shimizu, G. S. Simpson, P.-A. Söderström, H. Watanabe, F. Browne, P. Doornenbal, G. Gey, H. S. Jung, B. Meyer, T. Sumikama, J. Taprogge, Zs. Vajta, J. Wu, H. Baba, 1 G. Benzoni, K. Y. Chae, F. C. L. Crespi, N. Fukuda, R. Gernhäuser, N. Inabe, T. Isobe, T. Kajino, D. Kameda, G. D. Kim, Y.-K. Kim, I. Kojouharov, F. G. Kondev, T. Kubo, N. Kurz, Y. K. Kwon, G. J. Lane, Z. Li, A. Montaner-Pizá, K. Moschner, F. Naqvi, M. Niikura, H. Nishibata, A. Odahara, R. Orlandi, Z. Patel, Zs. Podolyák, H. Sakurai, H. Schaffner, P. Schury, S. Shibagaki, K. Steiger, H. Suzuki, H. Takeda, A. Wendt, A. Yagi, and K. Yoshinaga, Phys. Rev. Lett. **114**, 192501 (2015).

[29] R. Dunlop, V. Bildstein, I. Dillmann, A. Jungclaus, C. E. Svensson, C. Andreoiu, G. C. Ball, N. Bernier, H. Bidaman, P. Boubel, C. Burbadge, R. Caballero-Folch, M. R. Dunlop, L. J. Evitts, F. Garcia, A. B. Garnsworthy, P. E. Garrett, G. Hackman, S. Hallam, J. Henderson, S. Ilyushkin, D. Kisliuk, R. Krücken, J. Lassen, R. Li, E. MacConnachie, A. D. MacLean, E. McGee, M. Moukaddam, B. Olaizola, E. Padilla-Rodal, J. Park, O. Paetkau, C. M. Petrache, J. L. Pore, A. J. Radich, P. Ruotsalainen, J. Smallcombe, J. K. Smith, S. L. Tabor, A. Teigelhöfer, J. Turko, and T. Zidar, Phys. Rev. C **93**, 062801(R) (2016).

[30] A. Jungclaus, H. Grawe, S. Nishimura, P. Doornenbal, G. Lorusso, G. S. Simpson, P.-A. Söderström, T. Sumikama, J. Taprogge, Z. Y. Xu, H. Baba, F. Browne, N. Fukuda, R. Gernhäuser, G. Gey, N. Inabe, T. Isobe, H. S. Jung, D. Kameda, G. D. Kim, Y.-K. Kim, I. Kojouharov, T. Kubo, N. Kurz, Y. K. Kwon, Z. Li, H. Sakurai, H. Schaffner, Y. Shimizu, K. Steiger, H. Suzuki, H. Takeda, Zs. Vajta, H. Watanabe, J. Wu, A. Yagi, K. Yoshinaga, G. Benzoni, S. Bönig, K. Y. Chae, L. Coraggio, J.-M. Daugas, F. Drouet, A. Gadea, A. Gargano, S. Ilieva, N. Itaco, F. G. Kondev, T. Kröll, G. J. Lane, A. Montaner-Pizá, K. Moschner, D. Mücher, F. Naqvi, M. Niikura, H. Nishibata, A. Odahara, R. Orlandi, Z. Patel, Zs. Podolyák, and A. Wendt, Phys. Rev. C **94**, 024303 (2016).

[31] P. Möller, J. R. Nix, and K.-L. Kratz, At. Data Nucl. Data Tables **66**, 131 (1997).

[32] I. N. Borzov, Nucl. Phys. A **777**, 645 (2006).

[33] I. N. Borzov, J. J. Cuenca-García, K. Langanke, G. Martínez-Pinedo, and F. Montes, Nucl. Phys. A **814**, 159 (2008).

[34] T. Marketin, L. Huther, and G. Martínez-Pinedo, Phys. Rev. C **93**, 025805 (2016).

[35] M. T. Mustonen and J. Engel, Phys. Rev. C **93**, 014304 (2016).

[36] P. Möller, B. Pfeiffer, and K.-L. Kratz, Phys. Rev. C **67**, 055802 (2003).

[37] Q. Zhi, E. Caurier, J. J. Cuenca-García, K. Langanke, G. Martínez-Pinedo, and K. Sieja, Phys. Rev. C **87**, 025803 (2013).

[38] A. P. Severyukhin and H. Sagawa, Prog. Theor. Exp. Phys. **2013**, 103D03 (2013).

[39] A. Etilé, D. Verney, N. N. Arsenyev, J. Bettane, I. N. Borzov, M. Cheikh Mhamed, P. V. Cuong, C. Delafosse, F. Didierjean, C. Gaulard, Nguyen Van Giai, A. Goasduff, F. Ibrahim, K. Kolos, C. Lau, M. Niikura, S. Roccia, A. P. Severyukhin, D. Testov, S. Tusseau-Nenez, and V. V. Voronov, Phys. Rev. C **91**, 064317 (2015).

[40] P. Ring and P. Schuck, *The Nuclear Many Body Problem* (Springer, Berlin, 1980).

[41] F. Stancu, D. M. Brink, and H. Flocard, Phys. Lett. B **68**, 108 (1977).

[42] G. Colò, H. Sagawa, S. Fracasso, and P. F. Bortignon, Phys. Lett. B **646**, 227 (2007); **668**, 457(E) (2008).

[43] T. Lesinski, M. Bender, K. Bennaceur, T. Duguet, and J. Meyer, Phys. Rev. C **76**, 014312 (2007).
[44] A. P. Severyukhin, V. V. Voronov, and N. V. Giai, Phys. Rev. C **77**, 024322 (2008).
[45] S. J. Krieger, P. Bonche, H. Flocard, P. Quentin, and M. S. Weiss, Nucl. Phys. A **517**, 275 (1990).
[46] V. G. Soloviev, Kgl. Dan. Vid. Selsk. Mat. Fys. Skr. **1**, 238 (1961).
[47] J. Terasaki, J. Engel, M. Bender, J. Dobaczewski, W. Nazarewicz, and M. Stoitsov, Phys. Rev. C **71**, 034310 (2005).
[48] A. P. Severyukhin, V. V. Voronov, I. N. Borzov, and Nguyen Van Giai, Rom. J. Phys. **58**, 1048 (2013).
[49] J. Suhonen, *From Nucleons to Nucleus* (Springer-Verlag, Berlin, 2007).
[50] J. Engel, M. Bender, J. Dobaczewski, W. Nazarewicz, and R. Surman, Phys. Rev. C **60**, 014302 (1999).
[51] A. C. Pappas and T. Sverdrup, Nucl. Phys. A **188**, 48 (1972).
[52] C. L. Bai, H. Q. Zhang, H. Sagawa, X. Z. Zhang, G. Colò, and F. R. Xu, Phys. Rev. C **83**, 054316 (2011).
[53] F. Minato and C. L. Bai, Phys. Rev. Lett. **110**, 122501 (2013); **116**, 089902(E) (2016).
[54] P. Bonche, H. Flocard, and P. H. Heenen, Comput. Phys. Commun. **171**, 49 (2005).
[55] W. Ryssens, V. Hellemans, M. Bender, and P.-H. Heenen, Comput. Phys. Commun. **187**, 175 (2015).
[56] P. Sarriguren, Phys. Rev. C **91**, 044304 (2015).
[57] M. Martini, S. Péru, and S. Goriely, Phys. Rev. C **89**, 044306 (2014).
[58] M. Wang, G. Audi, A. H. Wapstra, F. G. Kondev, M. MacCormick, X. Xu, and B. Pfeiffer, Chin. Phys. C **36**, 1603 (2012).
[59] A. Jungclaus, L. Cáceres, M. Górska, M. Pfützner, S. Pietri, E. Werner-Malento, H. Grawe, K. Langanke, G. Martínez-Pinedo, F. Nowacki, A. Poves, J. J. Cuenca-García, D. Rudolph, Z. Podolyak, P. H. Regan, P. Detistov, S. Lalkovski, V. Modamio, J. Walker, P. Bednarczyk, P. Doornenbal, H. Geissel, J. Gerl, J. Grebosz, I. Kojouharov, N. Kurz, W. Prokopowicz, H. Schaffner, H. J. Wollersheim, K. Andgren, J. Benlliure, G. Benzoni, A. M. Bruce, E. Casarejos, B. Cederwall, F. C. L. Crespi, B. Hadinia, M. Hellström, R. Hoischen, G. Ilie, J. Jolie, A. Khaplanov, M. Kmiecik, R. Kumar, A. Maj, S. Mandal, F. Montes, S. Myalski, G. S. Simpson, S. J. Steer, S. Tashenov, and O. Wieland, Phys. Rev. Lett. **99**, 132501 (2007).
[60] S. Ilieva, M. Thürauf, Th. Kröll, R. Krücken, T. Behrens, V. Bildstein, A. Blazhev, S. Bönig, P. A. Butler, J. Cederkäll, T. Davinson, P. Delahaye, J. Diriken, A. Ekström, F. Finke, L. M. Fraile, S. Franchoo, Ch. Fransen, G. Georgiev, R. Gernhäuser, D. Habs, H. Hess, A. M. Hurst, M. Huyse, O. Ivanov, J. Iwanicki, P. Kent, O. Kester, U. Köster, R. Lutter, M. Mahgoub, D. Martin, P. Mayet, P. Maierbeck, T. Morgan, O. Niedermeier, M. Pantea, P. Reiter, T. R. Rodríguez, Th. Rolke, H. Scheit, A. Scherillo, D. Schwalm, M. Seidlitz, T. Sieber, G. S. Simpson, I. Stefanescu, S. Thiel, P. G. Thirolf, J. Van de Walle, P. Van Duppen, D. Voulot, N. Warr, W. Weinzierl, D. Weisshaar, F. Wenander, A. Wiens, and S. Winkler, Phys. Rev. C **89**, 014313 (2014).
[61] T. Kautzsch, W. B. Walters, M. Hannawald, K.-L. Kratz, V. I. Mishin, V. N. Fedoseyev, W. Böhmer, Y. Jading, P. Van Duppen, B. Pfeiffer, A. Wöhr, P. Möller, I. Klöckl, V. Sebastian, U. Köster, M. Koizumi, J. Lettry, and H. L. Ravn (the ISOLDE Collaboration), Eur. Phys. J. A **9**, 201 (2000).
[62] M. Danchev, G. Rainovski, N. Pietralla, A. Gargano, A. Covello, C. Baktash, J. R. Beene, C. R. Bingham, A. Galindo-Uribarri, K. A. Gladnishki, C. J. Gross, V. Yu. Ponomarev, D. C. Radford, L. L. Riedinger, M. Scheck, A. E. Stuchbery, J. Wambach, C.-H. Yu, and N. V. Zamfir, Phys. Rev. C **84**, 061306(R) (2011).
[63] R. L. Varner, J. R. Beene, C. Baktash, A. Galindo-Uribarri, C. J. Gross, J. Gomez del Campo, M. L. Halbert, P. A. Hausladen, Y. Larochelle, J. F. Liang, J. Mas, P. E. Mueller, E. Padilla-Rodal, D. C. Radford, D. Shapira, D. W. Stracener, J.-P. Urrego-Blanco, and C.-H. Yu, Eur. Phys. J. A **25**, 391 (2005).
[64] H. Watanabe, G. Lorusso, S. Nishimura, Z. Y. Xu, T. Sumikama, P.-A. Söderström, P. Doornenbal, F. Browne, G. Gey, H. S. Jung, J. Taprogge, Zs. Vajta, J. Wu, A. Yagi, H. Baba, G. Benzoni, K. Y. Chae, F. C. L. Crespi, N. Fukuda, R. Gernhäuser, N. Inabe, T. Isobe, A. Jungclaus, D. Kameda, G. D. Kim, Y. K. Kim, I. Kojouharov, F. G. Kondev, T. Kubo, N. Kurz, Y. K. Kwon, G. J. Lane, Z. Li, C.-B. Moon, A. Montaner-Pizá, K. Moschner, F. Naqvi, M. Niikura, H. Nishibata, D. Nishimura, A. Odahara, R. Orlandi, Z. Patel, Zs. Podolyák, H. Sakurai, H. Schaffner, G. S. Simpson, K. Steiger, H. Suzuki, H. Takeda, A. Wendt, and K. Yoshinaga, Phys. Rev. Lett. **111**, 152501 (2013).
[65] J. J. Cuenca-García, G. Martínez-Pinedo, K. Langanke, F. Nowacki, I. N. Borzov, and F. Montes, Eur. Phys. J. A **34**, 99 (2007).
[66] I. N. Borzov, in *Fission and Properties of Neutron-Rich Nuclei*, edited by J. H. Hamilton and A. V. Ramayya (World Scientific, Singapore, 2014), p. 530.
[67] H. Mach, D. Jerrestam, B. Fogelberg, M. Hellström, J. P. Omtvedt, K. I. Erokhina, and V. I. Isakov, Phys. Rev. C **51**, 500 (1995).
[68] K. Miernik, Phys. Rev. C **90**, 054306 (2014).